# Slope Descent using Plowing to Minimize Slip for Planetary Rovers

**Daniel Loret de Mola Lemus***
*Robotics Institute, Carnegie Mellon University, Pittsburgh, Pennsylvania 15213*
*e-mail: dloret@cmu.edu*
**David Kohanbash**
*Robotics Institute, Carnegie Mellon University, Pittsburgh, Pennsylvania 15213*
*e-mail: dkohanba@cmu.edu*
**Scott Moreland**†
*Robotics Institute, Carnegie Mellon University, Pittsburgh, Pennsylvania 15213*
*e-mail: smoreland@cmu.edu*
**David Wettergreen**
*Robotics Institute, Carnegie Mellon University, Pittsburgh, Pennsylvania 15213*
*e-mail: dsw@ri.cmu.edu*

Received 31 July 2013; accepted 14 February 2014

Steep slopes of unconsolidated material at planetary destinations of recent interest, such as craters and skylights, defy descent by rovers due to uncontrolled slip. This work proposes a novel method based on braking by plowing to arrest slip during descent maneuvers on planetary terrains. The method covers two fundamental maneuvers: direct descent and point-turning. For direct descent, an automatic control system estimates slip through visual odometry and actuates a plow accordingly. For point-turning, the plow is engaged as a point of rotation. Experimental results showed that the slip control system for direct descent kept slip within ±5% for slopes as steep as 31° and for different commanded driving speeds. In the point-turning tests, downhill displacement was less than 0.08 m on inclinations up to 30°. Thus, a plowing policy was developed that allows precise descent on extreme slopes by minimizing slip. As a result, this work expands current rover mobility and control capabilities. © 2014 Wiley Periodicals, Inc.

## 1. INTRODUCTION

Recent findings from orbiter data have resulted in a growing interest in exploring craters and skylights on other planetary bodies. However, the terrain conditions at these locations challenge current rover mobility and control capabilities. Studies based on data from NASA's satellites suggest the presence of water ice inside lunar craters (Colaprete et al., 2010; Thomson et al., 2012). To confirm these findings *in situ*, a robotic explorer must be able to cope with high levels of slip since these craters have slopes of 30°–40° covered with fine regolith (Figure 1) (Heiken, Vaniman, & French, 1991). Other geological depressions of high scientific interest are skylights (Figure 2). In Mars, for example, skylights can provide entrance to caves that are deemed promising places to search for life (Léveillé & Datta, 2010). Nevertheless, an initial reconnaissance mission would require a rover to drive on the skylight rim's dangerous slopes to gather better data on its geometry.

From the different approaches proposed for slope descent, wheeled locomotion has been tested both under relevant conditions on Earth and in actual space missions. Wettergreen et al. (2010) carried out thorough field testing of a four-wheeled rover called Scarab at lunar-analog sites. The active suspension of the robot proved useful while descending 10°–20° slopes by lowering its center of gravity. Outside Earth, the Mars Exploration Rovers have provided vast information about wheeled mobility on the red planet. The two robots, Spirit and Opportunity, drove over different types of terrain that ranged from soft soil to slippery crater walls (Maimone, Cheng, & Matthies, 2007).

Another approach for descending slopes is legged locomotion, which can better shift the robot's center of mass during the motion. One example is SCORPION, an eight-legged bio-mimetic walking robot designed to handle extreme terrain (Spenneberg & Kirchner, 2007). Cordes et al. (2010) employed this robot as a scout for sample retrieval from the interior of an artificial crater. Another walking

*Daniel Loret de Mola is currently with Vecna Technologies, Inc. at daniel.loret@vecna.com.
†Scott Moreland is currently with the Jet Propulsion Laboratory at scott.j.moreland@jpl.nasa.gov.

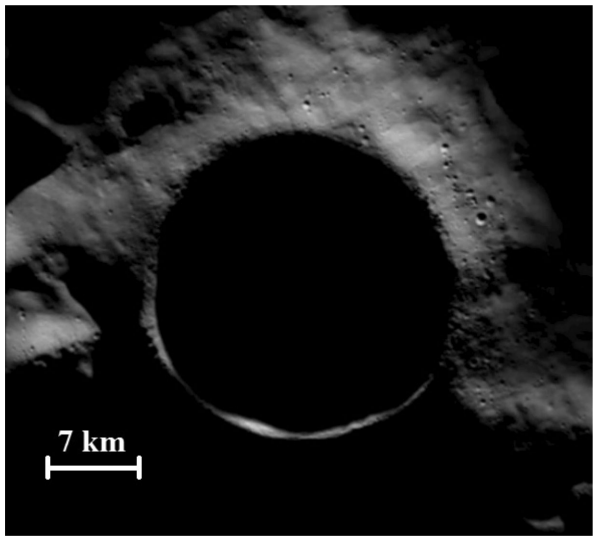


**Figure 1.** The Shackleton crater on the moon, with a diameter of 21 km and a depth of 4.2 km. The interior walls have an average grade of 31°. Scientists believe water ice lies in these walls and at the bottom of the crater.

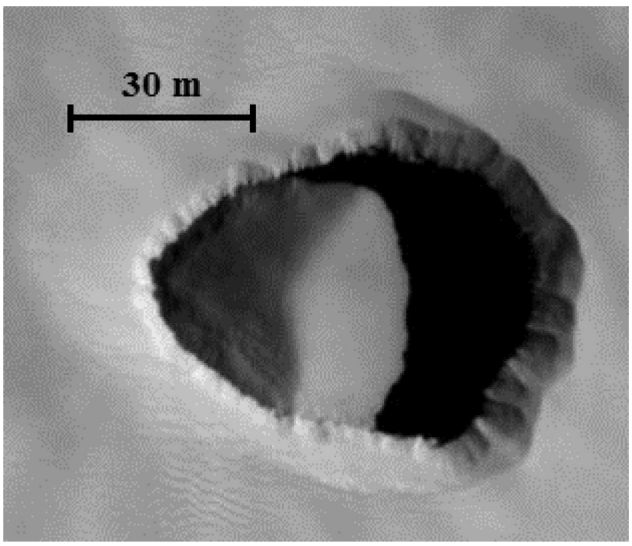


**Figure 2.** Fracture cave skylight on Mars. The entrance ledge of the pit slopes inward. A rover that can drive safely on the ledge would get a better view of the interior of the skylight.

robot, SpaceClimber, was partially inspired by SCORPION (Bartsch et al., 2012). The number of legs in SpaceClimber was set to six, instead of eight, with the aim of achieving a better compromise between stability, redundancy, energy consumption, and weight.

Wheeled or legged locomotion have also been coupled with tethering. A tether makes motion possible on very steep slopes and cliffs. Dante II is one of the pioneers within tethered robots (Bares & Wettergreen, 1999). This walking rappelling machine negotiated 20°–45° slopes while descending to the floor of a volcano's crater in Alaska. A more recent rover that uses a combination of wheeled locomotion and tethering is DuAxel (Nesnas et al., 2012). It is a four-wheeled modular system that can be decoupled into an anchor base and a rappelling rover with two wheels. The DuAxel system was field-tested on Mars analogue sites where it rappelled down near-vertical walls.

While each of the aforementioned locomotion concepts has particular advantages, there are some disadvantages associated with them. Although wheeled mobility technology has a good level of maturity now, it is not well-suited for steep slopes covered with soft soil. For instance, it took weeks to drive the Opportunity rover away from a big rock while descending Endurance Crater due to high slip on its 17°–23° slopes (Maimone et al., 2007). Legged robots have good climbing capability, but their high number of actuators makes them inconvenient for space applications where power is limited. SpaceClimber, for example, uses 24 actuators for its legs (Bartsch et al., 2012). Finally, rappelling robots can move along almost vertical slopes, however lateral motion is limited because the tether pulls in the opposite direction. This was one of the causes of Dante II's tipover during its ascent from Mount Spurr's crater (Bares & Wettergreen, 1999). Furthermore, when the slope is several kilometers long, such as in lunar craters (Heiken et al., 1991), unspooling tether is impractical due to payload mass and complexity.

Our rover platform, Icebreaker, uses tracked locomotion and plowing for enhanced mobility on steep slopes of unconsolidated material (Figure 3). The tracks offer forceful traction and high floatation on loose soil. The low center of gravity of the vehicle, 0.17 m from the ground, also improves its stability and slope-climbing capabilities.

**Figure 3.** Icebreaker rover. In this photograph, the plow (rod with point tip at the center of the vehicle) is about to engage the ground.

Additionally, the robot has a novel plowing instrument that boosts mobility on slopes of up to 38° (Ziglar, 2007). The instrument, here called the "plow," is an omnidirectional mechanism that can drive a daggerlike rod into the ground to provide a breaking force for the vehicle. The plow exploits the higher strength of the subsurface of loose, granular soil.

Previous research has focused on the validation of Icebreaker's configuration and braking by plowing (Kohanbash, Moreland, & Wettergreen, 2012; Ziglar, Kohanbash, Wettergreen, & Whittaker, 2008). However, how to best use the plow to reduce slip was left as an open question. Hence, the purpose of this study was to develop a plowing policy that nullifies the slip of the rover during descent on steep slopes of loose soil. This is of the utmost importance to keep the robot safe and maintain control authority while descending these slopes. Direct descent, point-turning, and cross-slope traversal are the basic maneuvers necessary to drive down to any point on a slope. Since lateral slip during cross-slope traversal can be mitigated well by the vehicle's configuration alone (Kohanbash et al., 2012), we propose specific plowing strategies for the other two driving scenarios. For direct descent, a vision system estimates vehicle slip, which in turn is regulated by closed-loop feedback control around the plow. For point-turning, the plow is engaged at maximum depth to serve as a pivot for rotation. The strategies were tested under lunar relevant conditions. The results show that slip was kept very low for both maneuvers on slopes of up to 31°.

## 2. TERRAMECHANICS OF TRACKED LOCOMOTION AND BRAKING BY PLOWING

Before presenting the different plowing strategies and the corresponding experimental results, the basic underlying terramechanics principles of our tracked rover and its plowing mechanism are introduced in this section. There are two types of interactions between soil and a track: tractive/braking effort and motion resistance. The tractive/braking effort is the thrust/braking force produced when the track shears the soil. Motion resistance comprises the forces exerted by the terrain opposite to the motion of the track due mainly to soil compaction and bulldozing. Additionally, the plowing mechanism generates a braking force that can be analyzed by regarding the instrument as a narrow tine dragged at a certain depth. The aforementioned forces are depicted in Figure 4.

The tractive/braking effort can be expressed in terms of slip, and also depends on soil and vehicle parameters. The slip of a track is defined as

$$i = \frac{V_T - V}{V_T} = \frac{V_j}{V_T} \tag{1}$$

where $V$ is the track's actual forward speed, $V_T$ is the circumferential speed of the track belt, and $V_j$ is the speed of slip of the track with respect to the ground. When $V_j$ is positive, the track is in driving state and thrust is generated. When it is negative, the track is in braking state and braking force is produced. For both cases, the force can be expressed as follows (Wong, 2001):

$$F = (blc + W\ \tan\phi)\left[1 - \frac{K}{l|i|}(1 - e^{-l|i|/K})\right]\text{sign}(i) \tag{2}$$

where $b$ and $l$ are the width and length of the track, respectively; $W$ is the normal load; $c$, $\phi$, and $K$ are the apparent cohesion, the angle of internal shearing resistance, and the shear deformation modulus of the soil, respectively; and sign($i$) is 1 if $i > 0$, $-1$ if $i < 0$, and 0 if $i = 0$. The experiments presented in this paper were performed on GRC-1 lunar simulant for which $c \approx 0$ kPa, $\phi = 33.3°$, and $K = 0.0255$ m (Oravec, Zeng, & Asnani, 2010).

There are some important remarks on Eq. (2). First, the equation assumes loose soil, a rigid track, and uniform normal pressure distribution. These assumptions are sensible given Icebreaker's configuration and the testing conditions. Second, in this work, the definition of slip in Eq. (1) is allowed to take negative values. In this way, Eq. (2) does not need to be redefined in terms of skid, $(V_T - V)/V$, when the track is in braking state, which is useful when a dynamic model of the robot is programmed for simulations (Loret de Mola Lemus, 2013).

Motion resistance forces can be represented by a longitudinal resistance $R$ and a lateral resistance distribution $R_l$, as shown in Figure 4. These resisting forces can be expressed in terms of constant coefficients of friction (Bekker, 1956; Wong, 2001). The longitudinal resistance $R$ acts

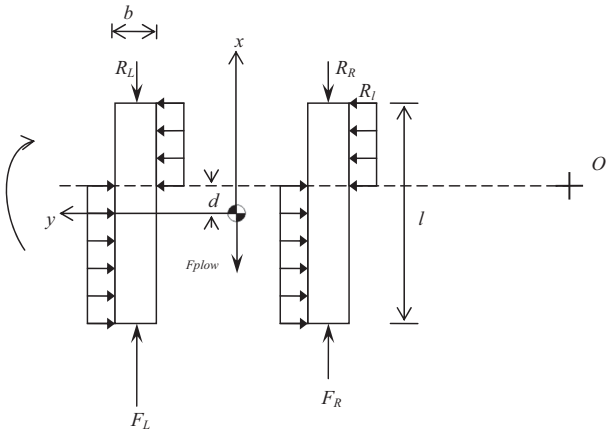


**Figure 4.** Free body diagram of the robot. The diagram corresponds to a top view of the rover while turning around $O$ on leveled ground. The $x$ axis points toward the vehicle's front. The displacement $d$ of the center of rotation is necessary so that the force distribution $R_l$ accelerates the vehicle toward $O$. Forces $R_i$ and $F_{\text{plow}}$ resist the motion in the longitudinal direction, while $F_i$ represents track thrust ($i$ denotes the side in which the track is).

opposite to the direction of the longitudinal motion of the track. Its magnitude is

$$R = f_r \cdot W \tag{3}$$

where $f_r$ is a longitudinal friction coefficient. The lateral resistance distribution $R_l$ is caused by sideslip of the vehicle. Its intensity is

$$R_l = \mu_t \frac{W}{l} \tag{4}$$

where $\mu_t$ is a lateral friction coefficient. Typical values for $f_r$ and $\mu_t$ of a tracked vehicle on sandy terrain are 0.1 and 0.5, respectively (Wong, 2001).

The braking force generated by the robot's plow is associated with the failure modes of the soil around the dragged instrument. Making the analogy with a narrow tine (Godwin & Spoor, 1977), when the plow depth, measured from ground level toward the plow's tip, is below a so-called critical depth, crescent failure occurs above the critical depth, and lateral failure develops below it. Crescent failure is characterized by brittle soil failure, which does not provide a significant resistance force. On the other hand, lateral failure compacts the soil in the direction of motion, which results in a greater resistance force (Godwin, 2007). Hence, plow depth must be below the critical depth to exploit the subsurface strength. Given Icebreaker's low speeds, the braking force from the added effect of crescent and lateral failures can be expressed in terms of plow depth as follows (Godwin & O'Dogherty, 2007):

$$F_{plow} = a_0 + a_1 \cdot depth + a_2 \cdot depth^2 \tag{5}$$

where the coefficients $a_0$, $a_1$, and $a_2$ depend on soil parameters, the plow's geometry, and geometric measurements, such as critical depth, that describe the failure patterns. For Icebreaker's plow, critical depth is around 0.05 m.

In summary, the rover acts on the terrain through its tracks and plowing mechanism. Track-soil interactions include tractive/breaking effort and motion resistance. Plow-soil interaction is determined by the way in which the soil fails around the dragged instrument. The description of both types of interactions gives a general understanding of the fundamental principles of Icebreaker's tracked locomotion and breaking by plowing.

## 3. DIRECT DESCENT

This section covers the plowing strategy for direct descent, the scenario in which the robot drives down-slope in a straight line along the steepest direction. First, Section 3.1 presents a set of experiments in which, throughout a run, the plow depth was kept constant. The corresponding results make evident the necessity of actively controlling the plow's depth while the rover is driving. Hence, Section 3.2 explains the development and field testing of a slip control system built around the plow.

One definition of slip used in this section is instantaneous slip. It is expressed as

$$i_{vehicle} = \frac{V_T - \dot{x}}{V_T} \tag{6}$$

where $\dot{x}$ is the actual forward speed of the robot's center of gravity and $V_T$ is the circumferential speed of the track belts. The latter can be obtained from the driving sprockets' encoder readings and is also referred to as commanded speed throughout this paper. Analogous to Eq. (1), the value of Eq. (6) is allowed to be negative. If the skid definition, $(V_T - \dot{x})/\dot{x}$, were used when $\dot{x} > V_T$, skid would be nonlinear with respect to $\dot{x}$ for a given $V_T$. On the other hand, if only Eq. (6) is used, slip is linear with respect to $\dot{x}$ whether $\dot{x}$ is greater or less than $V_T$. The benefit of this is that the error signal of the slip controller presented in Section 3.2.1 is also linear with respect to $\dot{x}$.

The second definition of slip used in this section is total slip. Its expression is

$$i_{total} = \frac{D_T - D}{D_T} \tag{7}$$

where $D$ is the vehicle's actual down-slope displacement and $D_T$ is the theoretical displacement derived from the circumferential speed of the track belts. Equations (6) and (7) can be expressed in percentage form by multiplying by 100.

The objective of the plowing strategy for direct descent is to minimize slip in the absolute sense. Negative slip should be avoided because the robot could slide uncontrollably. Also, positive slip is undesirable since part of the vehicle's tractive effort is wasted overcoming the plow's breaking force.

### 3.1. Fixed-depth Plowing

This section presents two groups of tests relevant to direct descent in which the plow was fixed at some depth for any given run. Their purpose is to explore the effect of static plowing in vehicle slip. The first group consisted of executing direct descents on a slope of 31° at different plow depths. The second group was a series of drawbar pull tests with the plow at various depths. The latter gave a rough idea of the robot's ability to descend on different terrain grades. All experiments were performed on lunar regolith simulant. The experimental design for each type of test is explained first in Section 3.1.1. Then, Section 3.2.2 analyzes the results.

#### 3.1.1. Experimental Design

All the experiments presented in this paper were conducted at the NASA Glenn Research Center (GRC), where lunar relevant terrain conditions can be attained. The tests described in this section took place at GRC's Simulated Lunar Operations (SLOPE) facility. The description of the experimental

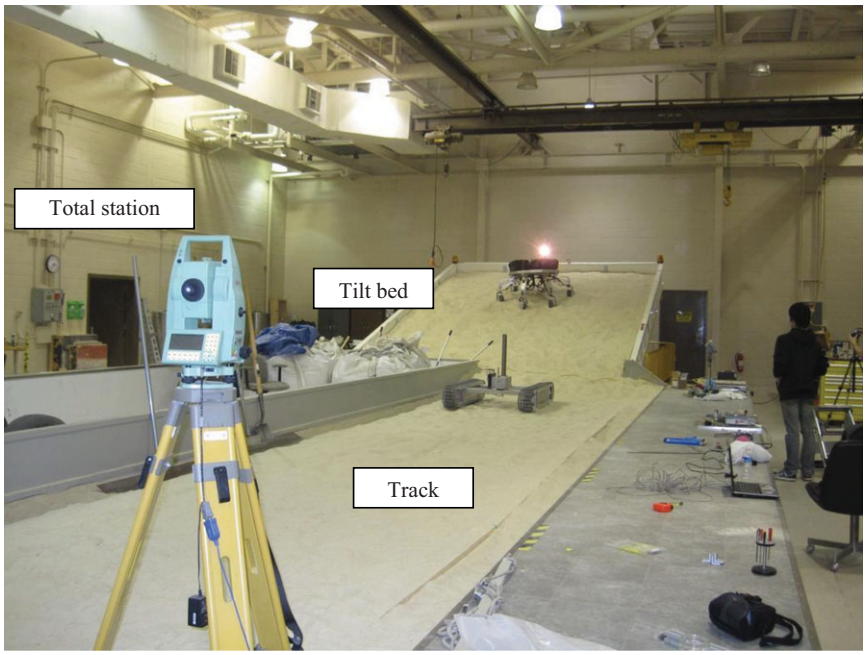


**Figure 5.** NASA GRC's SLOPE facility. The picture shows Icebreaker on the track section.

setup is given next, followed by the testing procedures carried out: descent on an inclinable platform and drawbar pull.

The SLOPE facility has a large sandbox with adjustable slope, here called the tilt bed, and a long track next to it (Figure 5). Both are filled with GRC-1 lunar simulant (Oravec et al., 2010). Before each experiment, the soil is prepared using a standard method called T3 (Woodward, 2011). This process involves using a shovel to disturb and loosen the subsurface soil where the rover will be operating. Then, it is smoothed lightly with a rake to insure uniform conditions for the test. As a consequence, the terrain is loose enough to provide a high slip scenario. To compute the vehicle's slip, measurements from a Leica TCRA1103+ total station and encoder readings from the robot's driving sprockets are logged. The total station generates position data by tracking a prism mounted on the rover. The instrument has a precision of 5 mm and less than 0.0014°. If speed data is needed, such as the robot's actual forward speed in Eq. (6), the timestamps of the position data are used. The drawbar pull tests also use an adjustable load system that applies a pulling force to the vehicle through a cable. A load cell is hooked between the test apparatus' cable and the robot in order to measure the actual load applied.

The first group of experiments was direct descent on the tilt bed set at 31° (Figure 6). In each run, the robot was commanded to drive 1 m down-slope with the plow kept at a constant depth. The commanded forward speed of the robot was 0.051 m/s. There were a total of four runs that used 0, 0.07, 0.14, and 0.20 m plow depths, respectively. The plow is disengaged at a depth of 0 m, and 0.20 m corresponds to maximum depth. Total slip, defined in Eq. (7), was computed in each test by comparing the commanded 1 m displacement against the actual translation measured by the total station.

**Figure 6.** Direct descent test on tilt bed at 31°. This picture shows a descent run with the plow disengaged.

The second group of tests involved a series of drawbar pull experiments. Again, a drawbar run was conducted for each plow depth: 0, 0.07, 0.14, and 0.20 m. Each test was


**Figure 7.** Harnessing the robot in drawbar pull tests. The adjustable load system's cable is pulled in the direction of motion of the vehicle.

performed as follows. First, the robot was placed at one end of the facility's track section, and its front was tied to the cable of the adjustable load system as shown in Figure 7. Then, the robot was commanded to advance along a straight line at 0.051 m/s. While driving, the cable pulled the robot in the direction of motion. The pulling force was increased at fixed intervals of time. During each interval the force was constant, and several instantaneous slip measurements were computed with Eq. (6).

The next section summarizes and discusses the results of the tilt bed and drawbar pull tests.

### 3.1.2. Experimental Results and Discussion

This section analyzes the results of direct descents on the tilt bed and drawbar pull experiments. The tilt bed tests exhibit the effect on slip of static plowing for a given terrain inclination. On the other hand, a general idea of the impact on slip of static plowing across various slope grades can be inferred from the drawbar pull experiments. For this, the pull coefficient will be associated with the slope angle. The pull coefficient is defined as the ratio between the drawbar pull force and the vehicle's weight (Freitag, 1965). The arctangent of the pull coefficient will be calculated to obtain the inclination angle. This assumes that the pulling force emulates the component of gravity along the direction of motion in a descent. However, it is important to note that this pull coefficient–slope angle association is only made to perform rough analyses, because in reality the relation is much more complex.

In the tests on the tilt bed at 31°, the deeper the plow was engaged, the less negative the total slip became. This behavior is shown in Figure 8, which plots the total slip measured for each of the plow depths tested. Total slip was negative without using the plow. As plow depth increased,

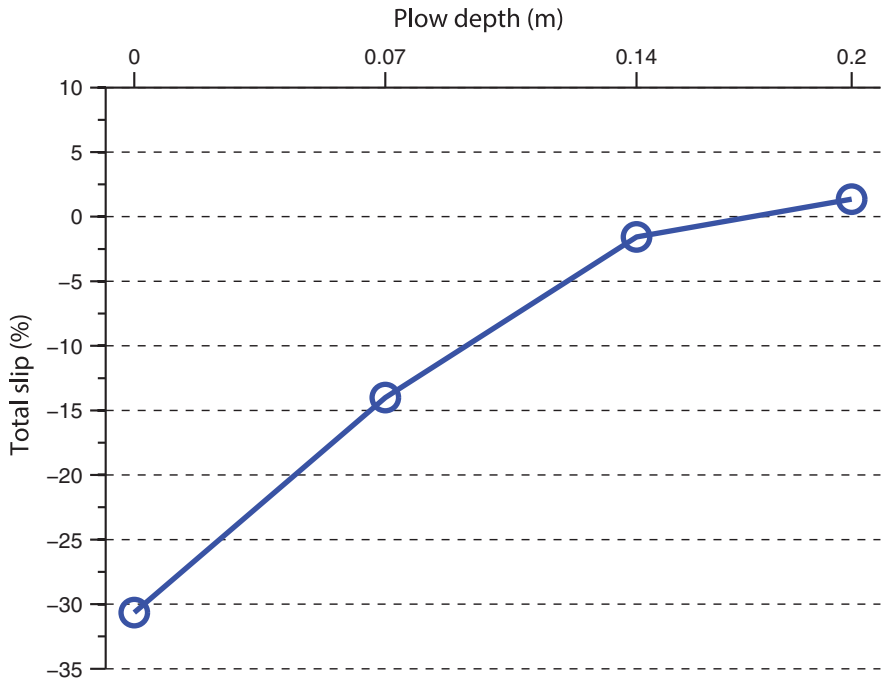


**Figure 8.** Direct descent test results on tilt bed at 31° with GRC-1. Plow depths tested were 0, 0.07, 0.14, and 0.20 m. For 0.14 m, total slip was −1.57%, while for 0.20 m, it was 1.37%.

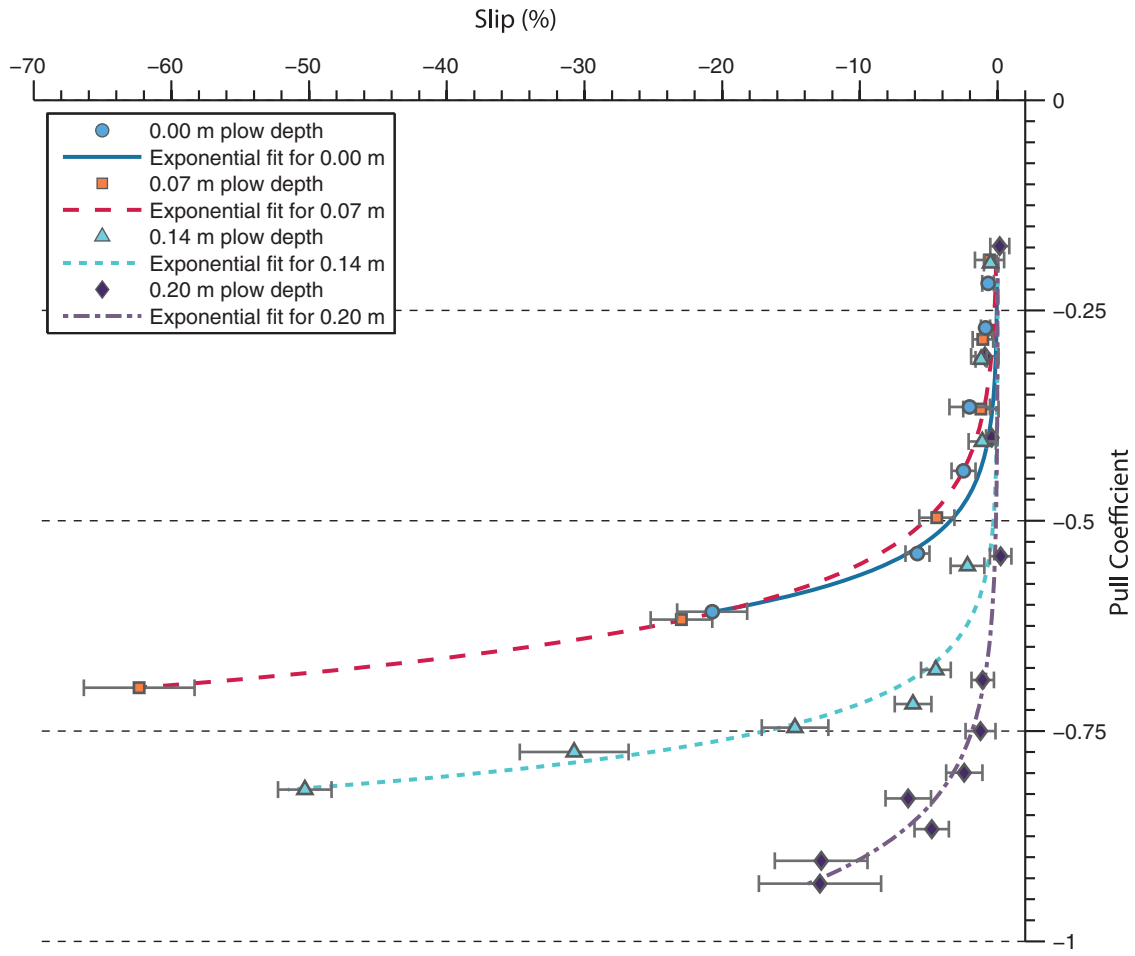


**Figure 9.** Drawbar pull test results for four plow depths on GRC-1. Instantaneous slip is plotted against pull coefficient, the ratio between drawbar pull, and vehicle weight. The error bars are calculated from the standard error of the slip measurements for a given drawbar load. Every slip mean is computed from 4 to 10 measurements. Each curve is fitted to all its corresponding slip measurements. For a pull coefficient around −0.75, which would be roughly equivalent to a 37° descent, the plow depth of 0.20 m was the only one that kept the average slip in the order of −1%. However, for a pull coefficient of approximately −0.2 (~11° descent), this same depth produced positive slip. At this coefficient, a 0.07 m plow depth resulted in an average of −0.58% slip.

slip decreased in magnitude until it finally became positive at a depth of 0.20 m. The largest tested plow depth that still yielded negative total slip was 0.14 m. This suggests that the optimum depth that drives slip to zero during a direct descent on a 31° slope of GRC-1 might be between 0.14 and 0.20 m.

In general, the drawbar pull test results were that a particular plow depth's effectiveness in keeping instantaneous slip near zero varied across different inclinations. Figure 9 plots the instantaneous slip against the pull coefficient for the four plow depths tested. Based on the explanation given before about the relation between pull coefficient and slope angle, it can be observed from the figure that at an inclination around 37° [−0.75 pull coefficient, $\tan^{-1}(0.75) \approx 37°$], only a 0.20 m plow depth is able to keep negative slip small in the absolute sense. However, at an inclination of approximately 11° (−0.2 pull coefficient), this depth generates positive slip. In this case, a small plow depth such as 0.07 m is appropriate. This indicates that for every GRC-1 terrain grade, there is some plow depth that will adequately arrest slip.

From these results, it is evident that there is no specific plow depth that will reduce slip across all terrain grades. In other words, different plow depths are better suited to different inclinations. Furthermore, a set of drawbar pull curves is specific to a given soil and soil state such as compaction level. As a consequence, the optimal plow depth depends not only on the terrain grade, but also on the soil

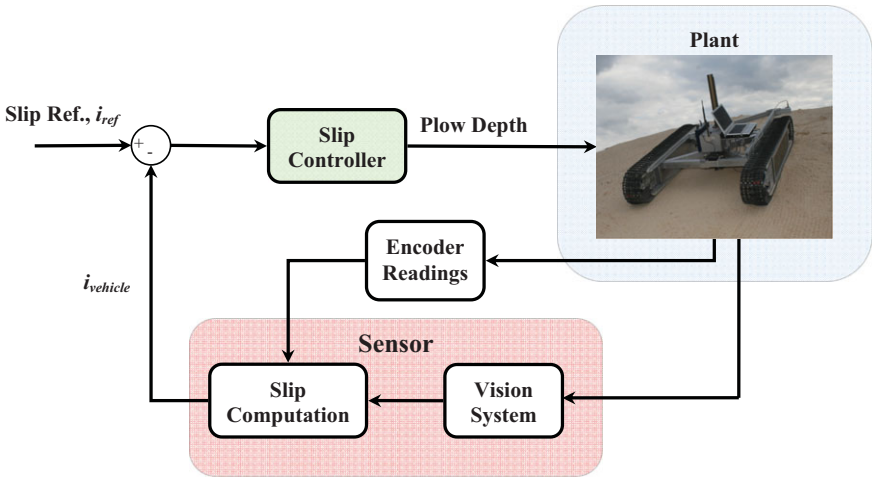


**Figure 10.** Diagram block representation of the slip control system. The flow of information in the system is depicted by arrows.

and its state. This suggests that the ability to dynamically set the depth of the plow based on the perceived vehicle slip is necessary to effectively minimize it. The next section develops this idea in the form of a slip control system with closed-loop feedback.

### 3.2. Dynamic-depth Plowing for Slip Control

The strategy for direct descent proposed in this paper is dynamic-depth plowing, which is to actively modify the plow's depth based on the estimated instantaneous slip. To implement it, a slip control system was developed. The control system's components are the plant, the controller, the sensor, and the signals. A block diagram representation is shown in Figure 10.

The interrelation between the components is as follows. The plant is the vehicle-terrain system. The plant's input is plow depth. The output of the plant is the actual forward speed of the robot. The sensor estimates this speed, compares it with the driving sprockets' encoder data, and computes slip. The sensor is comprised by a vision system and the application of Eq. (6). The plant and the sensor together form the process. The controller's law is a proportional-integral-derivative (PID) algorithm. Its input is the error signal computed as the difference between the set point, which is zero, and the estimated slip. Its output is the commanded plow depth.

The vision system encompasses a camera, a visual odometry algorithm based on monocular optical flow, and outlier rejection and filtering of the algorithm's estimates. This system estimates the forward speed of the robot's center of gravity at an average frequency of 12 Hz. The camera has a resolution of 640×480 pixels, a frame rate of 60 frames per second (FPS), and a field of view of 96.25×71.85°. The visual odometry algorithm is computationally efficient, uses pyramidal Lucas-Kanade feature tracking, and applies

**Figure 11.** Vision system's camera. The camera is mounted far enough from the track so that the imaged sand remains mainly static.

shadow rejection (Seegmiller & Wettergreen, 2011). The output estimates of the algorithm go through outlier rejection (Menold, Pearson, & Allgower, 1999) and low-pass filtering.

The main assumptions of the visual odometry algorithm are locally flat terrain and consistent local terrain orientation with respect to the camera. The first assumption is reasonably met since the imaged region is small. The second one is normally met except in abrupt transitions of the terrain's geometry (e.g., transition from slope to leveled ground). Mounting the camera behind the robot's left track, as seen in Figure 11, helps the algorithm in several ways. First, it contributes to the first assumption by flattening the terrain before it is imaged. Another advantage is that the track marks left behind offer excellent features to track.

The slip controller component is explained in Section 3.2.1. Then, Section 3.2.2 presents the experimental results

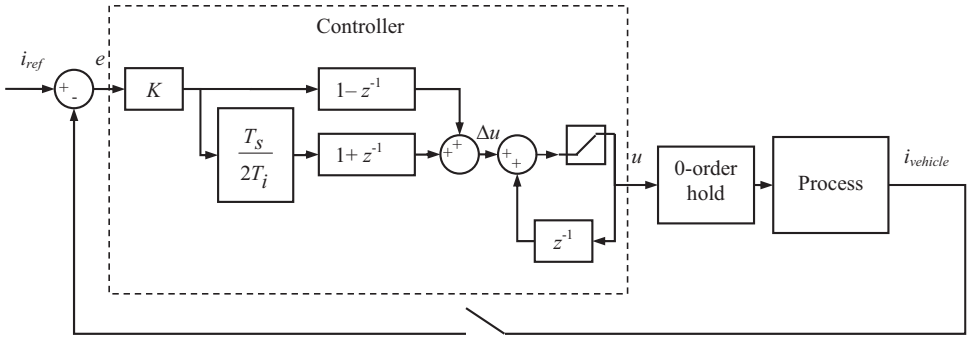


**Figure 12.** Block diagram of PI control system. Transfer functions are expressed as $z$ transforms. Incremental output $\Delta u$ enters a saturation loop to keep the commanded plow depth $u$ within 0–0.20 m. A zero-order hold is used to make $u$ a continuous signal, and vehicle slip $i_{\text{vehicle}}$ is sampled before computing slip error $e$.

of the slip control system tested on slopes relevant to lunar crater exploration.

### 3.2.1. Slip Controller

To develop the controller, the control problem was formally defined, then a control law was selected, and finally the parameters of the law's equation were tuned. The control problem was formulated by delimiting the process to regulate and establishing performance objectives. A PID algorithm was chosen for the law because PID control has been applied successfully to a wide variety of applications. The tuning was performed through simulations.

The definition of the control problem consisted of designating the components and signals of the control system, and setting forth performance objectives. The designation was presented in Section 3.2, and it resulted in a system that controls a single-input single-output (SISO) process. The input of the process is plow depth, and its output is instantaneous slip. The core of the performance objectives was to keep slip within ±5%, here called the allowable band, for different slope grades and commanded forward speeds of the robot.

The control law selected is based on a velocity form of the digital PID controller described by Seborg, Mellichamp, and Thomas (1986). The mathematical expression of the law is

$$\Delta u[k] = K\left((e[k]-e[k-1]) + \frac{T_s}{T_i}\left(\frac{e[k]+e[k-1]}{2}\right) + \frac{T_d}{T_s}(e[k]-2e[k-1]+e[k-2])\right) \quad (8)$$

where $\Delta u$ is the increment in plow depth, $e$ is the error in slip ($i_{\text{ref}} - i_{\text{vehicle}}$), $K$ is the proportional gain, $T_i$ is the integral time, $T_d$ is the derivative time, and $T_s$ is the sampling period. The derivative action in the law was discarded for the final implementation of Eq. (8) given the results of parameter tuning, as explained next.

The parameters $K$, $T_i$, and $T_d$ were tuned by performing simulations with a dynamic model of the vehicle-terrain system (Loret de Mola Lemus, 2013). The model is based on the principles presented in Section 2. The procedure involved setting custom bounds on specific signals, and optimizing the parameters through several runs of a 31° descent simulation until the bounds were satisfied. The selection of the bounds aimed to meet the performance objectives. After the optimization, the values of the parameters were $K = 0.0246$, $T_i = 0.0948$, and $T_d = 0.00058 \approx 0$. Hence, the resulting controller was PI. The sampling time was set to 0.5 s, which gives the plow enough time to reach the commanded position before the next control cycle starts. A block diagram representation of the final implementation of the control system is depicted in Figure 12.

To validate that the designed slip control system met the established performance goal, a series of experiments were carried out on lunar-analog terrain with different inclinations. Section 3.2.2 presents these tests.

### 3.2.2. Experimental Results and Discussion

A series of experiments were carried out at NASA Glenn Research Center to corroborate that the performance goal stated in Section 3.2.1 was met by the implemented slip control system. One group of tests was executed at the SLOPE facility, and another at the Dunes outdoor rover-testing site. In general, it was found that the proposed system was able to arrest slip for different terrain grades and commanded speeds, and to cope with some deviations from the visual odometry's assumptions.

Some conventions were followed for the figures in this section. First, the robot's driving sprockets were already spinning at the commanded angular velocity in each plot. In other words, the acceleration transitions of the sprockets when the rover is commanded to start moving and to stop are not shown. Second, slip curves are plotted with small circles centered on the discrete measurements. Third, the

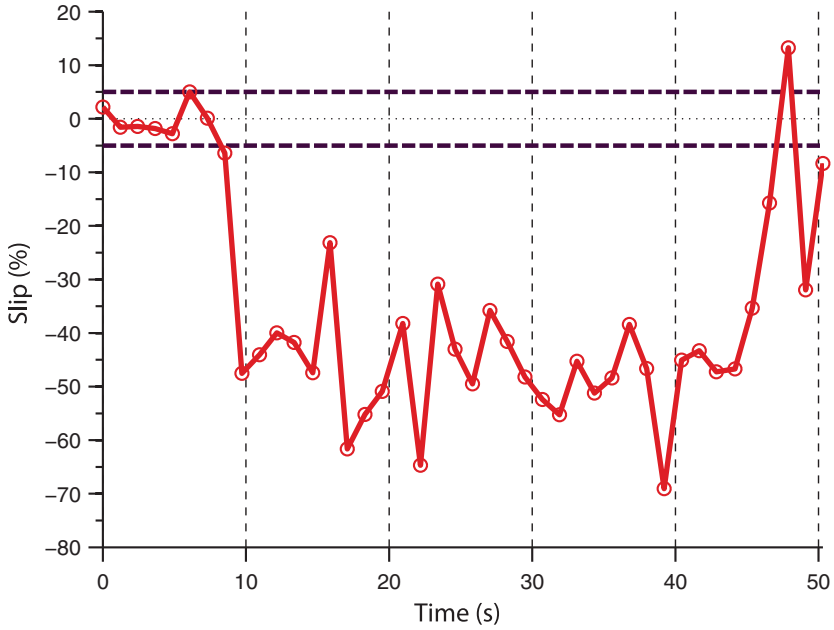


**Figure 13.** Descent on 31° slope at 0.037 m/s without slip control. Significant negative slip caused by a landslide starts developing around 9 s.

allowable band is depicted as dashed bold lines in the slip plots.

To put the experimental results into context, an example of a descent without automatic slip control is presented first. In this experiment, the tilt bed was set to 31° and the plow was not engaged. The robot was commanded to descend along a straight line with a forward speed of 0.037 m/s. As in Section 3.1.1, the total station's measurements were used to compute the actual forward speed in the vehicle slip formula, Eq. (6). The slip undergone by the robot is shown in Figure 13. Slip values were around −50% with some values reaching up to −70%. Therefore, the robot slid considerably when no slip control was in place.

The experiments at the SLOPE facility were aimed at testing the performance of the control system in arresting slip during direct descent for different terrain grades and various commanded speeds. Hence, in all experiments a zero slip reference was selected. The experimental setup was similar to the one described for the direct descent tests of Section 3.1.1. In particular, GRC-1 soil, T3 soil preparation, and a total station for ground truth data were used. Here, the tilt bed was set to 20°, 25°, and 31°, and the commanded forward speeds of the robot were 0.024, 0.037, and 0.049 m/s. Each run consisted in a combination of one of the slopes with one of the speeds. All possible combinations were tested. Below, representative results of the experiments are given. Each figure has three plots. The topmost shows vehicle slip computed with the robot's actual forward speed estimated by the vision system. The middle shows plow depth. The bottom presents the speed estimated by the vision system and its ground truth derived from the total station's measurements. Analogous to Section 3.1.1, the total station's position data and its timestamps are used to compute the ground truth speed.

The action of the slip control system while the robot was driving down a slope of 31° at a commanded speed of 0.037 m/s is shown in Figure 14. The system only took around 4.7 s to drive slip within the allowable band. After the signal reached the band, the few slip points that went outside the band were near its borders, and were quickly brought back inside. Furthermore, most of the slip measurements were very close to zero.

Figure 15 shows the performance of the control system on a slope of 25° at a commanded speed of 0.049 m/s. The controller required around 8.5 s to get the slip signal into the allowable band. Once the slip was inside the band, it mostly remained there. In two instances, the signal crossed the borders, but the controller corrected the situation in an acceptable time. As in the previous experiment, slip was centered on zero throughout most of the run.

Finally, a test that involved a slope of 20° and a commanded speed of 0.024 m/s is presented in Figure 16. Slip entered the allowable band after 9 s. It remained there except for a few small spikes that the controller handled well. Once again, the controller kept the slip signal centered on zero.

In summary, the control system was able to successfully drive slip into the allowable band quickly for different

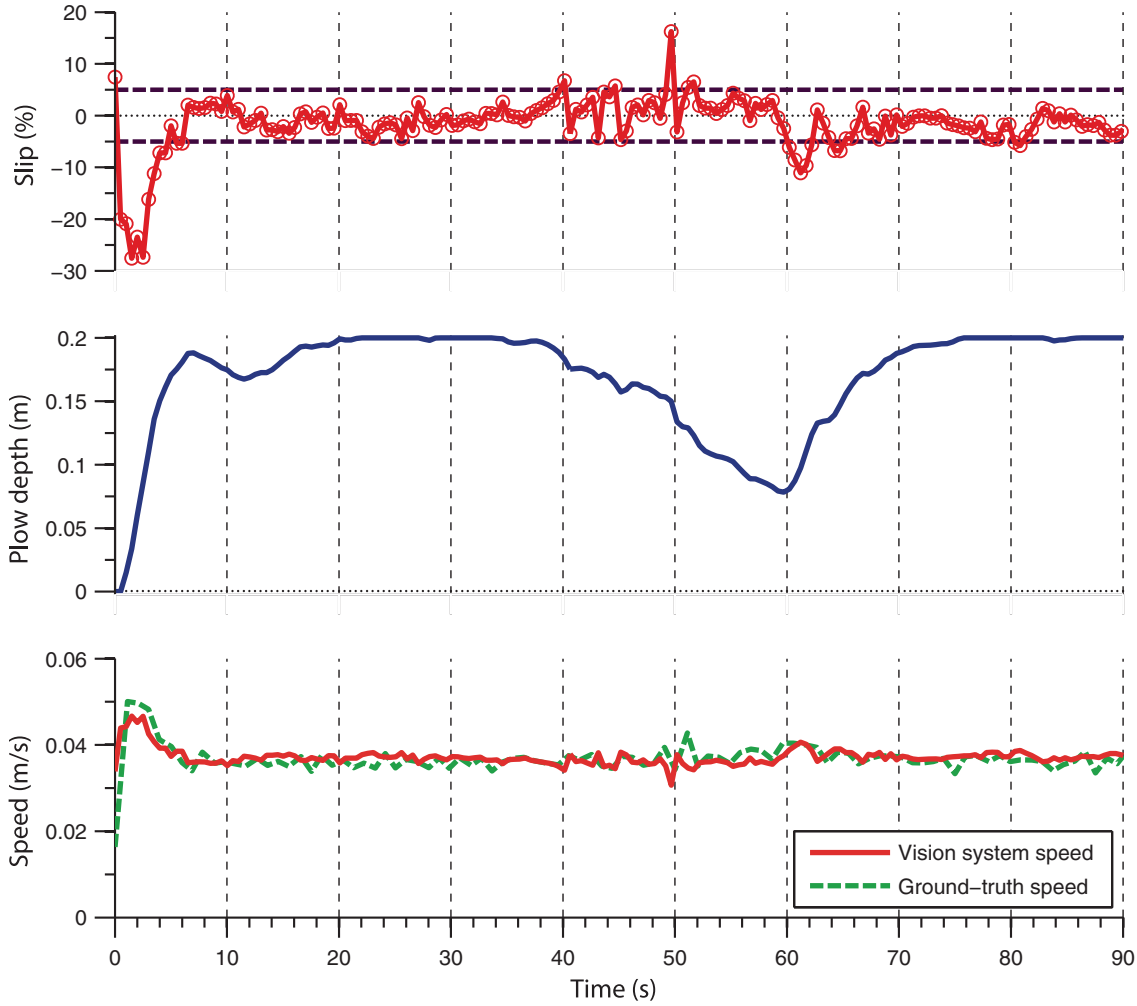


**Figure 14.** PI regulating slip on 31° slope at 0.037 m/s. An initial high value of negative slip was counteracted by a fast increase in plow depth.

terrain slopes and at various commanded speeds. The results also demonstrate that the slip values were kept near zero.

The other group of experiments was carried out at the Dunes (Figure 17). The site has a maximum slope grade of 20°, and GRC-1 makes up most of the soil's constitution there. The natural geometry of the Dunes made it possible to assess the performance of the slip control system when the visual odometry's assumptions are not fully met. In many of these tests, positive slip was registered most of the time. This was mainly because the slope was only 20°, and the soil was somewhat compacted from rain that occurred on the preceding days. Although a total station was not available at the site, errors of the vision system were evident during drastic transitions of the terrain geometry (e.g., when the robot moved from the top of the dune into the slope). While driving on the slope, however, the speed readings seemed reasonable, and the performance of the control system was acceptable. The experiment that had negative slip is presented here.

The results of a direct descent on the 20° side of the dune at a commanded speed of 0.049 m/s are shown in Figure 18. The slip entered the band in 1.7 s. A good amount of slip points were inside the band. Most of the points that were outside were above the band, as expected from the terrain conditions. As a consequence, the plow was inactive during a long period of the run. Nevertheless, the control system reacted appropriately when negative slip occurred.

The tests at the Dunes showed that the slip control system works reasonably well when the deviations from the assumptions of the visual odometry are small, but the performance decreases to some extent compared to the

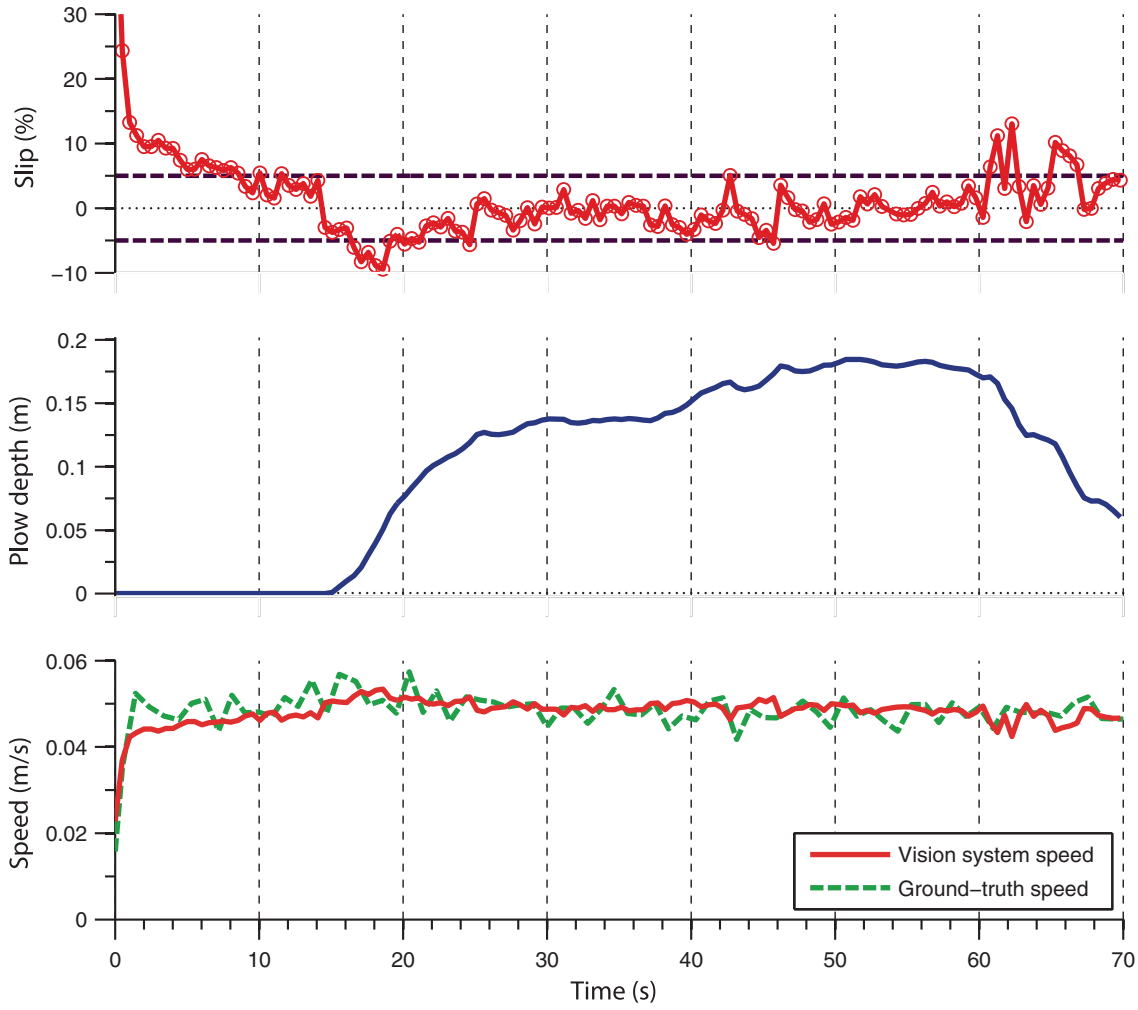


**Figure 15.** PI regulating slip on 25° slope at 0.049 m/s. The plow depth was zero during the beginning because the vision system was estimating positive slip.

results from the SLOPE facility. This dependence on the vision system comes from the fact that slip, Eq. (6), is directly calculated with the speed estimate. So if the estimates have a considerable error, the control system's performance will be affected significantly. This happened when the robot moved from the slope to the top/bottom of the dune or vice versa, which violated the assumption of a consistent local plane's orientation. But if the assumptions are only partly violated, the system can cope with the resulting inaccuracies. This was the case when the rover drove on the slope of the dune, where the assumption of the terrain's local flatness was partially met. The experiment shown corresponds to the latter case.

To recapitulate, the results of the experiments presented in this section demonstrate that the slip control system implemented for direct descent maneuvers satisfactorily minimizes slip. The system is effective for different terrain grades and commanded speeds, and can cope with small deviations from the visual odometry algorithm's assumptions.

## 4. POINT-TURNING

During point-turning on a slope, the plow serves as a pivot for rotation and acts against any other motion. The plow functions as a pivot because it is mounted near the robot's center of gravity. Therefore, it counteracts downhill motion that results from the weight of the robot and landslides. For any in-place turn, the plowing force acts opposite to the robot's weight component along the fall line of the slope. Furthermore, the plow serves as an anchor during landslides of surface soil dislodged by the turning tracks.

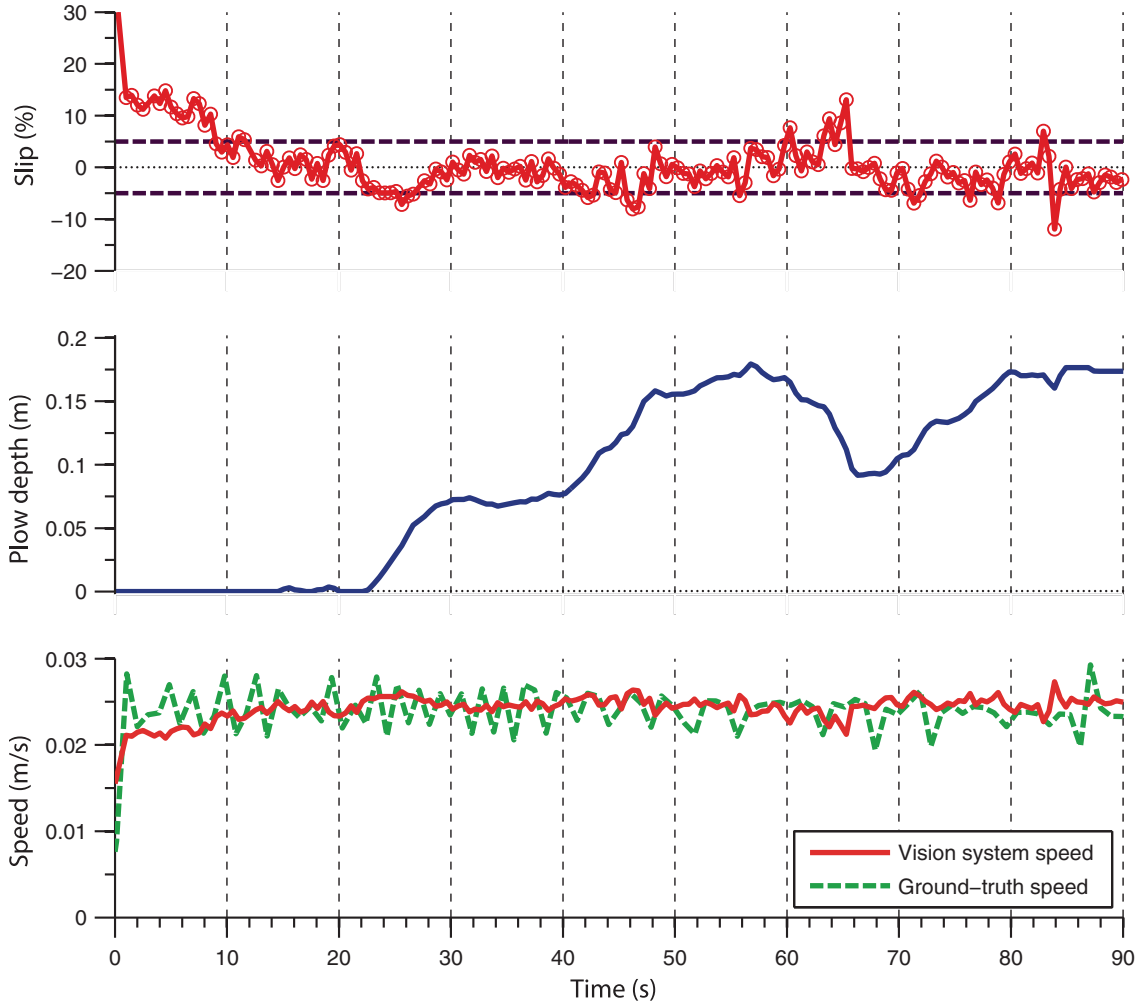


**Figure 16.** PI regulating slip on 20° slope at 0.024 m/s. The slip spike around 83 s was caused by noise in the estimated speed signal.

Based on the results of point-turn experiments performed with different plow depths, it was determined that the best strategy for point-turning is to engage the plow at the maximum allowable depth, in this case 0.20 m. The experimental procedure that was carried out is explained in Section 4.1. The results of the tests are analyzed in Section 4.2.

### 4.1. Experimental Design

Once again, the experiments took place on the tilt bed in the SLOPE facility. The experimental setup was similar to the one described in Section 3.1.1, which involved the use of GRC-1 soil, T3 soil preparation, and a total station to record position data. Here, the tilt bed was set to 10°, 15°, 20°, 25°, and 30°, and the plow depth to 0, 0.07, 0.14, and 0.20 m. Each test consisted in a combination of one of the slopes with one of the plow depths. For every run, the robot started with an orientation perpendicular to the downhill direction, as shown in Figure 19(A). Then, it was commanded to turn in place 90° in order to face the downhill direction [Figure 19(B)]. Slip was quantified by measuring the total downhill displacement at the end of the test.

### 4.2. Experimental Results and Discussion

The results of the point-turn experiments are shown in Figure 20. It is evident from the figure that across all the terrain grades, the point-turns using the maximum plow depth (0.20 m) had the lowest downhill displacement values. The reduction in slip by increasing plow depth was noticeable even at low inclinations. For example, on a slope of 15° the slip in a turn using a 0.20 m plow depth

**Figure 17.** NASA GRC's Dunes testing site. The picture shows the 20° side of the main dune with Icebreaker at the starting position of a test.

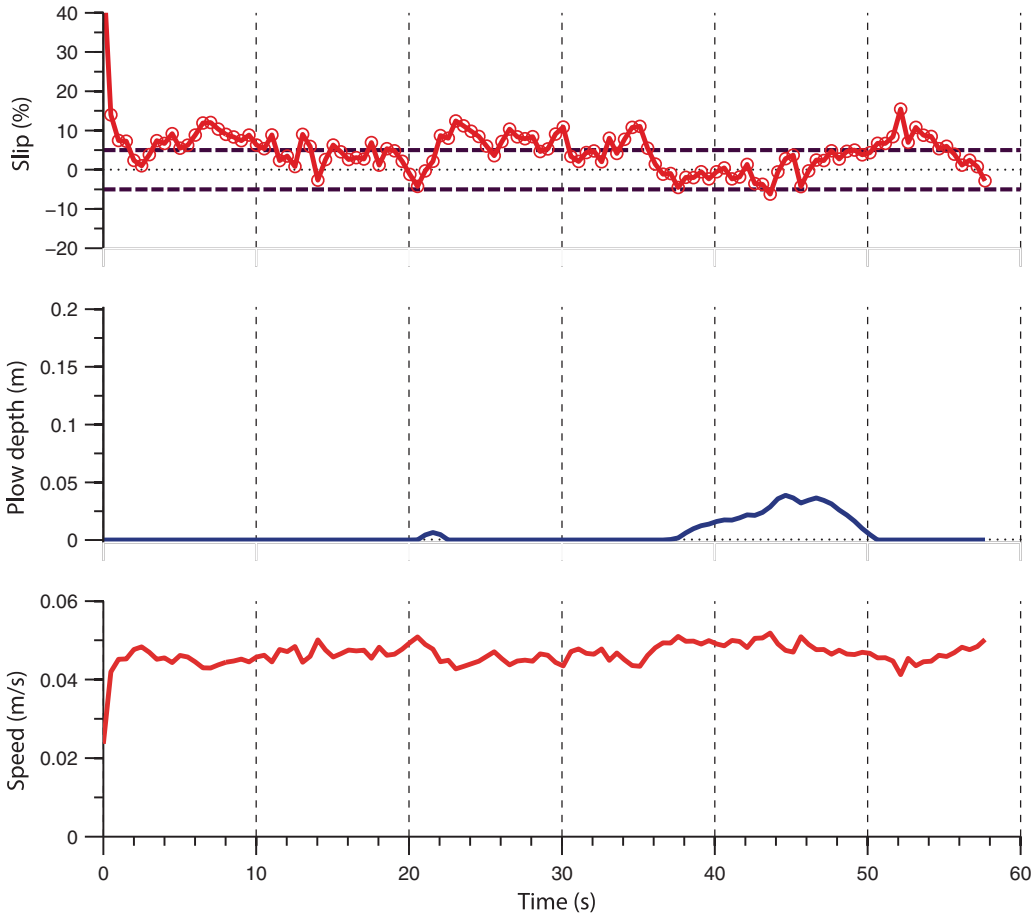


**Figure 18.** PI regulating slip in Dunes. The bottom plot corresponds to the robot's speed estimated by the vision system. When the robot started experiencing negative slip in the interval between 38 and 50 s, approximately, the controller correctly counteracted this by actuating the plow.


**Figure 19.** Point-turn test on GRC-1. The robot starts at the position shown in (A). Then it turns in place 90° to reach the final position shown in (B).

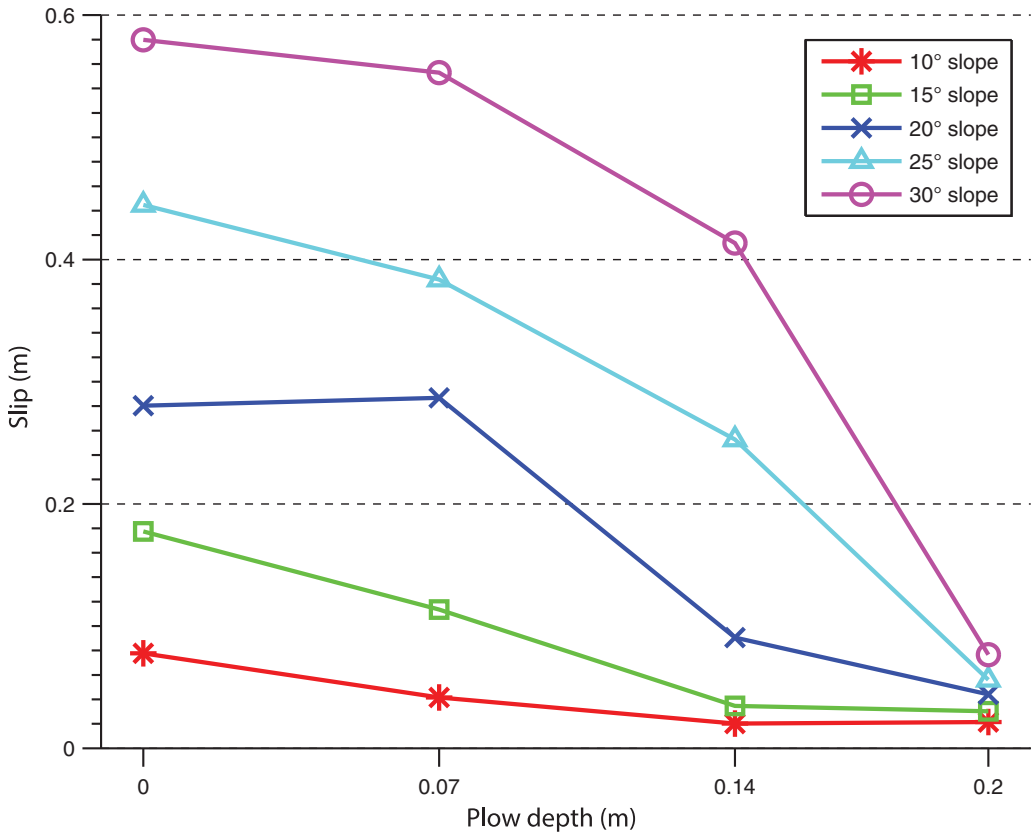


**Figure 20.** Point-turn test results on GRC-1. For a 15° slope, a point-turn with the plow disengaged resulted in 0.18 m of downhill displacement, while with the plow at 0.20 m, the displacement was 0.03 m. On a 30° slope, the robot slid 0.41 m with the plow at 0.14 m. However, with the plow at 0.20 m, the downhill displacement was 0.08 m.

was almost six times lower than turning without the plow. Even increasing the plow depth from 0.14 to 0.20 m had a positive impact, especially at steeper slopes. At 30°, for instance, the displacement after in-place turning with the plow at 0.20 m was 0.08 m, five times lower than the one experimented when turning with a 0.14 m plow depth.

As can be seen from the previous results, engaging the plow at the maximum allowable depth permits

point-turning with very small downhill displacement. It can also be observed that as the slope becomes steeper, the positive effect of plow depth is greater.

## 5. CONCLUSIONS

The objective of this research was to develop a policy for operating the plow of a rover to minimize slip during descent on steep slopes of unconsolidated material. From the results of the strategies proposed, the policy achieved its purpose. First, the slip control system implemented for direct descent kept slip near zero for different terrain grades and commanded speeds, which shows that it allows precise down-slope movement on slopes up to 31° at the robot's available speeds. Second, the small down-slope displacement during point-turning with the plow at 0.20 m indicates that the engagement at maximum depth permits effective in-place turning. As can be seen from the analysis of the results from each driving scenario, a policy that takes full advantage of the plow to minimize slip during descent on extreme slopes has been developed.

The main contribution of this work is the design and validation of a descent method based on plowing, which, together with a vehicle's configuration that performs well in cross-slope traverse, allows a rover to get to any location on the face of a slope with excellent accuracy. This expands current rover mobility capabilities by augmenting the control authority on slopes where standard robots would slide uncontrollably. A step forward has been taken in the realization of technologies to reach scientific targets precluded from exploration. These targets can range from water ice on the walls of lunar craters to mineral outcrops in the craters of Mars.

Some directions in which the work presented here can be further improved are accommodation of subsurface rocks, inclusion of switchback maneuvers, and application of plowing to other locomotion architectures. A problem that might arise when using the plow is hitting or getting stuck in rocks. A load cell could be installed in the plow mechanism to detect this, and, with suitable signal analysis and mechanism control, corrective actions could be applied accordingly. Also, the proposed descent approach was to move downhill along the steepest direction, but less aggressive approaches such as switchback maneuvers exist. The inclusion of switchbacks might require the slip control system to operate on both plow and tracks. Lastly, it is important to validate the use of plowing to descend slopes for mobility methods different from tracked locomotion. Wheeled vehicles, for example, would also need to limit the moment generated by the plowing force in order to avoid excessive sinkage of the front wheels.

In summary, the adequate use of plowing can dramatically boost the descent capability of planetary rovers. With the plowing strategies presented here, slip levels are very low for both direct descent and point-turning maneuvers. Since slip is small, the vehicle can move on the slope safely and accurately. An improvement in rover mobility of this nature will be vital to access the challenging locations targeted for planetary exploration.

## ACKNOWLEDGMENTS

We acknowledge and appreciate the technical assistance of Colin Creager, Kyle Johnson, and Vivake Asnani at NASA Glenn Research Center. Experiments for this work were conducted in the Simulated Lunar Operations (SLOPE) and Dunes facilities at NASA Glenn Research Center. This research was supported by NASA under Grants No. NNX07AE30G and No. NNX13AD45A.

## REFERENCES

Bares, J. E., & Wettergreen, D. S. (1999). Dante II: Technical description, results, and lessons learned. The International Journal of Robotics Research, 18(7), 621–649.

Bartsch, S., Birnschein, T., Römmermann, M., Hilljegerdes, J., Kühn, D., & Kirchner, F. (2012). Development of the six-legged walking and climbing robot Space Climber. Journal of Field Robotics, 29(3), 506–532.

Bekker, M. G. (1956). Theory of land locomotion. Ann Arbor, MI: University of Michigan Press.

Colaprete, A., Schultz, P., Heldmann, J., Wooden, D., Shirley, M., Ennico, K., et al. (2010). Detection of water in the LCROSS ejecta plume. Science, 330(6003), 463–468.

Cordes, F., Ahrns, I., Bartsch, S., Birnschein, T., Dettmann, A., Estable, S., Haase, S., et al. (2010). LUNARES: Lunar crater exploration with heterogeneous multi robot systems. Intelligent Service Robotics, 4(1), 61–89.

Freitag, D. R. (1965). A dimensional analysis of the performance of pneumatic tires on soft soils (Tech. Rep. No. AEWES-TR-3-688). Vicksburg, MS: Army Engineer Waterways Experiment Station.

Godwin, R. J. (2007). A review of the effect of implement geometry on soil failure and implement forces. Soil and Tillage Research, 97(2), 331–340.

Godwin, R. J., & O'Dogherty, M. J. (2007). Integrated soil tillage force prediction models. Journal of Terramechanics, 44(1), 3–14.

Godwin, R. J., & Spoor, G. (1977). Soil failure with narrow tines. Journal of Agricultural Engineering Research, 22(3), 213–228.

Heiken, G. H., Vaniman, D. T., & French, B. M. (1991). Lunar sourcebook: A user's guide to the moon. New York: Cambridge University Press.

Kohanbash, D., Moreland, S. J., & Wettergreen, D. (2012). Plowing for rover control on extreme slopes. Paper presented at the 8th International Conference on Field and Service Robotics, Matsushima, Japan.

Léveillé, R. J., & Datta, S. (2010). Lava tubes and basaltic caves as astrobiological targets on Earth and Mars: A review. Planetary and Space Science, 58(4), 592–598.

Loret de Mola Lemus, D. (2013). Slip control during slope descent for a rover with plowing capability. Unpublished master's thesis, Carnegie Mellon University, Pittsburgh, PA.

Maimone, M., Cheng, Y., & Matthies, L. (2007). Two years of visual odometry on the Mars exploration rovers. Journal of Field Robotics, 24(3), 169–186.

Menold, P. H., Pearson, R. K., & Allgower, F. (1999). Online outlier detection and removal. In L. Mirking (ed.), 7th IEEE Mediterranean Conference on Control and Automation (pp. 1110–1133). Haifa, Israel: IEEE.

Nesnas, I. A., Matthews, J. B., Abad-Manterola, P., Burdick, J. W., Edlund, J. A., Morrison, J. C., et al. (2012). Axel and DuAxel rovers for the sustainable exploration of extreme terrains. Journal of Field Robotics, 29(4), 663–685.

Oravec, H. A., Zeng, X., & Asnani, V. M. (2010). Design and characterization of GRC-1: A soil for lunar terramechanics testing in Earth-ambient conditions. Journal of Terramechanics, 47(6), 361–377.

Seborg, D. E., Mellichamp, D. A., & Thomas, F. E. (1986). Process dynamics and control. Somerset, NJ: John Wiley & Sons.

Seegmiller, N., & Wettergreen, D. (2011). Optical flow odometry with robustness to self-shadowing. In N. Amato (ed.), 2011 IEEE/RSJ International Conference on Intelligent Robots and Systems (pp. 613–618). San Francisco, CA: IEEE.

Spenneberg, D., & Kirchner, F. (2007). The bio-inspired SCORPION robot: Design, control & lessons learned. In H. Zhang (Ed.), Climbing and walking robots, towards new applications (pp. 197–218). Vienna, Austria: I-Tech Education and Publishing.

Thomson, B. J., Bussey, D. B. J., Neish, C. D., Cahill, J. T. S., Heggy, E., Kirk, R. L., et al. (2012). An upper limit for ice in Shackleton crater as revealed by LRO Mini-RF orbital radar. Geophysical Research Letters, 39(14).

Wettergreen, D., Moreland, S., Skonieczny, K., Jonak, D., Kohanbash, D., & Teza, J. (2010). Design and field experimentation of a prototype lunar prospector. The International Journal of Robotics Research, 29(12), 1550–1564.

Wong, J. Y. (2001). Theory of ground vehicles (3rd ed.). New York: John Wiley & Sons.

Woodward, A. C. (2011). Experimental analysis of the effects of the variation of drawbar pull test parameters for exploration vehicles on GRC-1 lunar soil simulant. Unpublished master's thesis, Virginia Polytechnic Institute and State University, Blacksburgh, VA.

Ziglar, J. (2007). Rover configuration for exploring lunar craters. Unpublished master's thesis, Carnegie Mellon University, Pittsburgh, PA.

Ziglar, J., Kohanbash, D., Wettergreen, D., & Whittaker, W. (2008). Plowing for controlled steep crater descents. Paper presented at the International Symposium on Artificial Intelligence, Robotics and Automation in Space (iSAIRAS), Hollywood, CA.